

Kapitza-like Modulation of Near-Field Radiative Heat Transfer

Mauro Antezza^{1,2,*}

¹Laboratoire Charles Coulomb (L2C), UMR 5221 CNRS-Université de Montpellier, F-34095 Montpellier, France

²Institut Universitaire de France, 1 rue Descartes, Paris Cedex 05 F-75231, France

(Dated: May 19, 2026)

We introduce a Kapitza-like mechanism for the near-field radiative heat transfer and show that fast modulation of any parameter controlling the flux, such as the vacuum gap or a material response, produces a quadratic, time-averaged correction in the slow thermal dynamics. This correction splits into a frequency-independent static term and a low-pass dynamical term, yielding sizable modulation-induced temperature shifts and modified effective thermal conductances that can stabilize or destabilize the steady state. Applying the theory to gap modulation between SiC slabs, we derive analytical scaling laws and predict temperature shifts that are fully measurable with existing experimental platforms, requiring only readily accessible low modulation frequencies of order $\Omega \approx 10^4$ rad/s. Our results establish a thermal analogue of the Kapitza mechanism and provide a general route for controlling radiative heat flow in micro- and nanoscale platforms.

I. INTRODUCTION

High-frequency parametric excitation can stabilize otherwise unstable equilibria. This phenomenon, known as the Kapitza effect, was analyzed for an inverted pendulum with a rapidly oscillating pivot via a separation of slow and fast motions leading to an effective time-averaged potential [1, 2]. Averaging and Floquet ideas have since permeated many areas of physics [3–7]. In parallel, the past two decades have established the foundations and experimental reality of *near-field radiative heat transfer* (NFRHT), where thermally excited evanescent fields enable photon tunneling across subwavelength gaps, yielding heat fluxes far exceeding the blackbody limit [8–16]. Quantitative measurements down to nanometric gaps have confirmed the predictions of fluctuational electrodynamics across diverse materials and geometries [17–20]. These advances now enable dynamic control via electromechanical gap actuation or dispersion engineering [21, 22]. In this work we bring these two threads together and analyze how *fast* periodic modulation of a near-field coupling parameter modifies the *slow* thermal dynamics of a lumped body. In close analogy with Kapitza stabilization, averaging over fast oscillations yields an additional, state-dependent term in the slow equation of motion that can enhance the effective restoring conductance around an equilibrium and considerably affect the thermal state. This opens new modulation mechanisms in currently accessible experimental NFRHT platforms.

II. PHYSICAL SYSTEM

We consider two bodies (e.g., parallel plates, sphere-slab,...) where body 1 has a temperature $T(t)$ that evolves under the system's thermal balance, while body 2 is held at a fixed temperature T_2 , separated by a vacuum gap

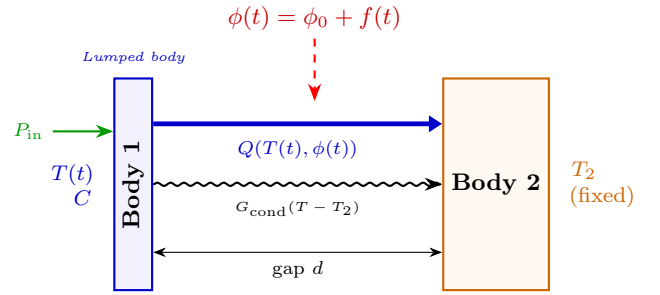


FIG. 1. Schematic of the lumped thermal system. Body 1 (the lumped body with heat capacity C and temperature $T(t)$) and Body 2 (a thicker reservoir at fixed T_2) are separated by a gap d . The energy exchange is composed of a radiative heat flux Q , dynamically modulated by a generic external parameter $\phi(t)$ at frequency Ω , and a background conductive channel G_{cond} .

d (see scheme in Fig.1). We assume each body remains at a uniform temperature, so body 1 can be treated as a lumped thermal mass with heat capacity per unit area C . It receives an external power flux P_{in} and loses heat through a background conductive channel $G_{cond}(T - T_2)$, where $G_{cond} > 0$ is the non-radiative thermal conductance per unit area to body 2 (or to the environment). The net radiative flux between the two bodies (W/m^2) is [8–11]

$$Q(T, \phi) = \int_0^\infty \frac{d\omega}{2\pi} \Phi(\omega, \phi) [\Theta(\omega, T) - \Theta(\omega, T_2)], \quad (1)$$

where $\Theta(\omega, T) = \hbar\omega / [\exp(\hbar\omega/k_B T) - 1]$, $\Phi(\omega, \phi) > 0$ is the spectral radiative transmission, and $\phi(t)$ is a generic time-dependent externally-modulated control variable (gap, material property, chemical potential, etc.) affecting the radiative coupling. The dynamics of $T(t)$ is then given by the balance equation:

$$C\dot{T}(t) = P_{in} - G_{cond}(T(t) - T_2) - Q(T(t), \phi(t)). \quad (2)$$

This model applies when the internal thermal resistance is negligible compared to external losses, as in thin membranes or small objects, so that the body equilibrates

* mauro.antezza@umontpellier.fr

internally much faster than it exchanges heat with its surroundings. We treat G_{cond} and C as temperature independent, since the small temperature oscillations considered here render their variations negligible relative to the nonlinear radiative term $Q(T, \phi)$.

We focus on fast and small modulations around a mean value ϕ_0 :

$$\phi(t) = \phi_0 + a \cos(\Omega t), \quad 0 < a \ll \phi_0, \quad \Omega \gg G/C. \quad (3)$$

This modulation induces fast temperature oscillations, motivating the decomposition

$$T(t) = \bar{T}(t) + \xi(t), \quad (4)$$

where $\bar{T}(t)$ is the *slow* component (varying on the slow timescale $\sim C/G$), defined as the average of $T(t)$ over one period of the fast drive $\bar{T}(t) = (\Omega/2\pi) \int_t^{t+2\pi/\Omega} T(t') dt'$, and $\xi(t)$ captures the small, *fast* oscillatory component (with a fast timescale $\sim 1/\Omega$, and average $\langle \xi \rangle = 0$ over one modulation period $2\pi/\Omega$). In Eq. (3) we also introduced the unmodulated effective conductance G evaluated at the average operating point (\bar{T}, ϕ_0) :

$$G(\bar{T}, \phi_0) = G_{\text{cond}} + G_{\text{rad}}(\bar{T}, \phi_0), \quad (5)$$

where $G_{\text{rad}}(\bar{T}, \phi_0) = Q_T(\bar{T}, \phi_0) \equiv \partial_T Q(T, \phi)|_{(\bar{T}, \phi_0)}$ is the unmodulated radiative conductance.

Let us now discuss the timescale requirements for the validity of this model. First, Kapitza-type averaging requires a separation of thermal and modulation timescales: the modulation period must be much shorter than the characteristic thermal relaxation time, i.e. $G/C \ll \Omega$. As we show below, this condition does not imply that the magnitude of the modulation-induced effects increases with Ω . Second, the use in (2) of the static near-field radiative heat flux $Q(T, \phi)$ evaluated at the instantaneous value of $\phi(t)$ is justified only when the electromagnetic field adjusts quasi-instantaneously to the modulation. This requires $\Omega \ll \gamma$, where γ is the spectral linewidth of the dominant evanescent modes, ω_{res} being the resonance frequency. A separate condition is that Ω must remain well below ω_{res} , since when Ω approaches ω_{res} , sideband generation and frequency-conversion effects become significant [22]. Together, all these constraints impose the double inequality $G/C \ll \Omega \ll \{\gamma, \omega_{\text{res}}\}$. For surface phonon polaritons in SiC, $\omega_{\text{res}} \approx 1.5 \times 10^{14}$ rad/s and $\gamma \sim 10^{11}$ – 10^{12} rad/s, both are several orders of magnitude above the modulation frequencies considered here.

III. FAST DYNAMICS

By inserting $T(t) = \bar{T}(t) + \xi(t)$ and $\phi(t)$ [Eq. (3)] into the thermal balance Eq. (2) and expanding the radiative flux to second order in ξ and a around (\bar{T}, ϕ_0) gives

$$\begin{aligned} C(\dot{\bar{T}} + \dot{\xi}) &= P_{\text{in}} - G_{\text{cond}}(\bar{T} + \xi - T_2) \\ &\quad - [Q_0 + Q_T \xi + \frac{1}{2} Q_{TT} \xi^2 + Q_{\phi} a \cos(\Omega t) \\ &\quad + Q_{T\phi} \xi a \cos(\Omega t) + \frac{1}{2} Q_{\phi\phi} a^2 \cos^2(\Omega t)], \quad (6) \end{aligned}$$

where $Q_0 = Q(\bar{T}, \phi_0)$ and $Q_{\alpha} = \partial_{\alpha} Q$ and $Q_{\alpha\beta} = \partial_{\alpha} \partial_{\beta} Q$ are evaluated at the same point.

To perform a two-scale analysis, we first isolate the fast dynamics by retaining terms that either depend on the fast variable ξ or oscillate at the modulation frequency Ω . Terms that vary slowly over a modulation period are effectively constant for the fast dynamics and can be neglected. Keeping only terms linear in ξ and a yields the equation for the fast component ξ :

$$C\dot{\xi} + G\xi = -Q_{\phi} a \cos(\Omega t). \quad (7)$$

This is a forced first-order system with sinusoidal forcing. Its homogeneous solution decays exponentially in time and is negligible in the steady state. We therefore focus only on the particular solution, which provides the steady periodic response:

$$\xi(t) = -\frac{Q_{\phi} a}{G^2 + (C\Omega)^2} [G \cos(\Omega t) + C\Omega \sin(\Omega t)]. \quad (8)$$

The temperature ripple $\xi(t)$ oscillates at the drive frequency Ω , with amplitude filtered by $[G^2 + (C\Omega)^2]^{-1}$ due to thermal inertia and conductance. Expressing $\xi(t)$ in polar form gives further insight:

$$\xi(t) = \frac{-Q_{\phi} a}{\sqrt{G^2 + (C\Omega)^2}} \cos(\Omega t - \varphi), \quad \tan \varphi = \frac{C\Omega}{G}. \quad (9)$$

In the frequency domain, writing $\cos(\Omega t) = \text{Re}[e^{i\Omega t}]$ and assuming a harmonic response $\xi(t) = \xi_{\Omega} e^{i\Omega t}$, equation (7) gives $\xi_{\Omega} = -H(i\Omega)[Q_{\phi} a]$, where $H(i\Omega) = 1/(G + iC\Omega)$ is a complex transfer function. Thus $1/\sqrt{G^2 + (C\Omega)^2}$ in (9) is the modulus of $H(i\Omega)$, representing the amplitude response, while the angle φ corresponds to the phase lag. Physically, G and C play roles analogous to resistance and capacitance in an RC circuit, so $\xi(t)$ acts as a thermal low-pass filter. Slow modulations of $\phi(t)$ ($\Omega \ll G/C$) are transmitted almost in phase [$\xi(t) \simeq -(Q_{\phi} a/G) \cos(\Omega t)$], so the temperature follows the modulation nearly instantaneously. Fast modulations ($\Omega \gg G/C$) are strongly attenuated ($\propto 1/\Omega$) and acquire a $\pi/2$ phase shift [$\xi(t) \simeq -(Q_{\phi} a/(C\Omega)) \sin(\Omega t)$] since the finite thermal inertia C delays the response. Hence, the factor $(G^2 + (C\Omega)^2)^{-1}$ in Eq. (8) simultaneously sets the amplitude reduction and the phase lag between forcing and thermal response.

IV. AVERAGED SLOW DYNAMICS

Averaging Eq. (6) over one modulation cycle using the fast solution (8) yields the slow dynamics of $\bar{T}(t)$:

$$\begin{aligned} C\dot{\bar{T}} &= P_{\text{in}} - G_{\text{cond}}(\bar{T} - T_2) - Q_0 \\ &\quad - \Delta_{\text{stat}}(\bar{T}) - \Delta_{\text{dyn}}(\bar{T}, \Omega), \quad (10) \end{aligned}$$

containing the Kapitza-like correction terms

$$\Delta_{\text{stat}} = \frac{a^2}{4} Q_{\phi\phi}, \quad (11)$$

$$\Delta_{\text{dyn}} = \frac{a^2}{4} \frac{Q_{TT} Q_{\phi}^2 - 2Q_{T\phi} Q_{\phi} G}{G^2 + (C\Omega)^2}, \quad (12)$$

with all quantities evaluated at (\bar{T}, ϕ_0) . Eq. (10) constitutes one of the central results of this work.

The static correction Δ_{stat} originates from the flux expansion term $\frac{1}{2} Q_{\phi\phi} a^2 \cos^2(\Omega t)$, which, when averaged over a cycle, produces a frequency-independent shift of the mean radiative load, modifying the baseline heat exchange without affecting the frequency response. The dynamic correction Δ_{dyn} arises from the interplay between the fast temperature ripple $\xi(t)$ and the modulation of the control parameter. It involves quadratic averages such as $\langle \xi^2 \rangle = (Q_{\phi a})^2 / [2(G^2 + (C\Omega)^2)]$ and $\langle \xi \cos \Omega t \rangle = -Q_{\phi a} G / [2(G^2 + (C\Omega)^2)]$. Through the filtering factor $1/[G^2 + (C\Omega)^2]$, Δ_{dyn} depends strongly on the modulation frequency, acting as a Kapitza-like correction that, as we will see, can either increase or decrease the effective thermal conductance. It vanishes at large Ω , so within the averaging regime ($\Omega \gg G/C$) it is largest at the lowest frequency compatible with time-scale separation.

At this stage $G(\bar{T}, \phi_0)$ is not required to be positive, since $\partial_T Q(T, \phi)|_{(\bar{T}, \phi_0)}$ can be negative; in systems with negative differential thermal conductance [23, 24], Eqs. (10)–(12) still hold.

V. STEADY-STATE MEAN TEMPERATURE SHIFT

To quantify the effect of the modulation, we compare the steady-state mean temperature T^* of the modulated system, obtained from Eq. (10):

$$0 = P_{\text{in}} - G_{\text{cond}}(T^* - T_2) - Q(T^*, \phi_0) - \Delta_{\text{stat}}(T^*) - \Delta_{\text{dyn}}(T^*, \Omega), \quad (13)$$

with the steady-state temperature T_0 of the unmodulated system:

$$0 = P_{\text{in}} - G_{\text{cond}}(T_0 - T_2) - Q(T_0, \phi_0). \quad (14)$$

Defining the stationary slow-temperature shift $\delta T^* = T^* - T_0$ and subtracting Eq. (14) from Eq. (13) one obtains

$$0 = -G_{\text{cond}} \delta T^* - [Q(T^*, \phi_0) - Q(T_0, \phi_0)] - \Delta_{\text{stat}}(T^*) - \Delta_{\text{dyn}}(T^*, \Omega). \quad (15)$$

For weak modulation (a small), expanding the flux to first order in δT^* as $Q(T^*, \phi_0) \simeq Q(T_0, \phi_0) + Q_T(T_0, \phi_0) \delta T^*$, and keeping only leading terms in δT^* and a^2 , we obtain the modulation-induced slow-temperature stationary shift

$$\delta T^* = - \frac{\Delta_{\text{stat}}(T_0) + \Delta_{\text{dyn}}(T_0, \Omega)}{G(T_0, \phi_0)}, \quad (16)$$

where $G(T_0, \phi_0) = G_{\text{cond}} + Q_T(T_0, \phi_0)$. Using Eqs. (11)–(12), this reads explicitly in terms of flux derivatives:

$$\delta T^* = - \frac{a^2}{4G} \left[Q_{\phi\phi} + \frac{Q_{TT} Q_{\phi}^2 - 2Q_{T\phi} Q_{\phi} G}{G^2 + (C\Omega)^2} \right], \quad (17)$$

with all quantities evaluated at (T_0, ϕ_0) . Here, T_0 itself depends on ϕ_0 via Eq. (14). The fast modulation hence produces an $O(a^2)$ shift of the time-averaged steady-state temperature δT^* , determined by the nonlinear derivatives of $Q(T, \phi)$ and the frequency-dependent factor contained in Δ_{dyn} .

This result is valid for small modulation amplitudes ($a \ll \phi_0$) and small temperature shifts: $|\delta T^*| \ll |T_0|$ and $|\delta T^*| \ll |T_0 - T_2|$. The latter condition ensures that the linear approximation of $Q(T, \phi)$ around T_0 remains valid and that T^* does not approach or cross T_2 , which would reverse the heat flux and invalidate the linearization. If the shift becomes comparable to the original temperature difference, the fully nonlinear system must be solved.

Regarding the sign of δT^* , let us consider the case of a vacuum-gap modulation ($\phi = d$). First, $G(T_0, \phi_0) > 0$ ensures that T_0 is a thermally stable steady state, an assumption required for the linearization leading to Eq. (16). Concerning the static contribution, in the near field $\Phi(\omega, d)$ typically decreases with d and is convex for small gaps, so that $\Phi_{dd} > 0$ and $Q_{dd} > 0$, yielding $\Delta_{\text{stat}} > 0$; the static term produces a negative mean temperature shift for the considered parameters. To study the dynamic correction, we note that $\Phi_d < 0$, and assuming $P_{\text{in}} > 0$ we also have $T_0 > T_2$, implying $Q_d < 0$ and $Q_{Td} < 0$. Since $\partial_T^2 \Theta > 0$, we have $Q_{TT} > 0$. Hence, the sign of Δ_{dyn} is determined by the relative magnitude of two contributions with opposite signs: $Q_{TT} Q_d^2 > 0$ and $-2Q_{Td} Q_d G < 0$.

VI. STABILITY UNDER MODULATION

If the averaged slow dynamics admits a stationary solution T^* , its stability is determined by considering small perturbations around T^* and linearizing the effective equation. Assuming $|\delta T| \ll T^*$ and $|\delta T| \ll |T^* - T_2|$, let us replace $\bar{T}(t)$ with $T^* + \delta T(t)$ into Eq. (10). Since T^* is a steady-state solution, it satisfies Eq. (13). Subtracting Eq. (13) from Eq. (10) and linearizing while retaining only terms linear in δT yields the perturbation equation:

$$C \delta \dot{T} = - \left[G(T^*, \phi_0) + \Delta G_{\text{eff}}(T^*, \Omega) \right] \delta T. \quad (18)$$

The term in brackets defines the *effective thermal conductance* of the modulated system

$$G_{\text{eff}}(T^*, \phi_0, \Omega) = G_{\text{cond}} + Q_T(T^*, \phi_0) + \Delta G_{\text{eff}}(T^*, \Omega), \quad (19)$$

and the (static and dynamic) Kapitza modulation-induced correction to the effective conductance is

$$\Delta G_{\text{eff}}(T^*, \Omega) = \partial_T [\Delta_{\text{stat}}(T) + \Delta_{\text{dyn}}(T, \Omega)] \Big|_{(T^*, \phi_0)}. \quad (20)$$

Equation (18) governs the evolution of small deviations $\delta T(t)$ from the stationary temperature T^* . The relaxation rate (stability exponent) of the exponential solution $\delta T(t) = \delta T(0)e^{-\lambda t}$ is $\lambda = G_{\text{eff}}(T^*, \phi_0, \Omega)/C$. Stability requires $G_{\text{eff}} > 0$, ensuring that perturbations decay exponentially. This behavior is the thermal analogue of the Kapitza effect in mechanics, where rapid oscillations generate an averaged stabilizing (or destabilizing) potential depending on the system parameters.

We note that even when the effective conductance $G_{\text{eff}} > 0$ stabilizes the averaged slow dynamics while $G < 0$, the full nonlinear time-dependent system may still exhibit instabilities beyond the validity of the averaging approximation.

VII. GAP MODULATION BETWEEN PARALLEL PLATES

The main equations above apply to any modulation parameter. As an illustrative case, we consider a gap modulation $\phi = d$. We also use the near-field radiative flux approximation:

$$Q(T, d) = \alpha(d)(T^m - T_2^m), \quad \alpha(d) = \frac{A}{d^n} > 0, \quad (21)$$

with typically $m \in [1, 3]$, $n \in [2, 4]$ [9, 10, 20, 25–28] where n and m depend on distances, temperatures, materials, and geometries of the involved bodies. This power-law form allows closed-form expressions for all quantities of interest, and its three parameters can be determined by fitting the computed or measured flux $Q(T, d)$.

Using (21), the static correction (11) becomes

$$\Delta_{\text{stat}}(T) = \frac{n(n+1)}{4} \left(\frac{a}{d}\right)^2 \alpha(d)(T^m - T_2^m), \quad (22)$$

which, being positive, enhances the damping of temperature deviations in (16). Using $Q_d = \alpha' S$, $S = T^m - T_2^m$, $Q_{TT} = \alpha m(m-1)T^{m-2}$, and $Q_{Td} = mT^{m-1}\alpha'$, Eq. (12) yields

$$\Delta_{\text{dyn}}(T, \Omega) = \frac{n^2(a/d)^2\alpha(d)^2}{4D(T)} F(T), \quad (23)$$

with $D(T) = G(T)^2 + (C\Omega)^2$, $G(T) = G_{\text{cond}} + \alpha m T^{m-1}$ and $F(T) = \alpha m(m-1)T^{m-2}S(T)^2 - 2mT^{m-1}S(T)G(T)$.

Using the model (21), the explicit expression for the thermal conductivity shift can be directly derived. The static shift of the effective conductance reads

$$\partial_T \Delta_{\text{stat}}|_{(T^*, d_0)} = \frac{n(n+1)}{4} \left(\frac{a}{d_0}\right)^2 \alpha(d_0) m T^{*m-1}. \quad (24)$$

This term is independent of the drive frequency Ω and provides a positive, stabilizing correction to the effective conductance. The dynamic conductance shift is

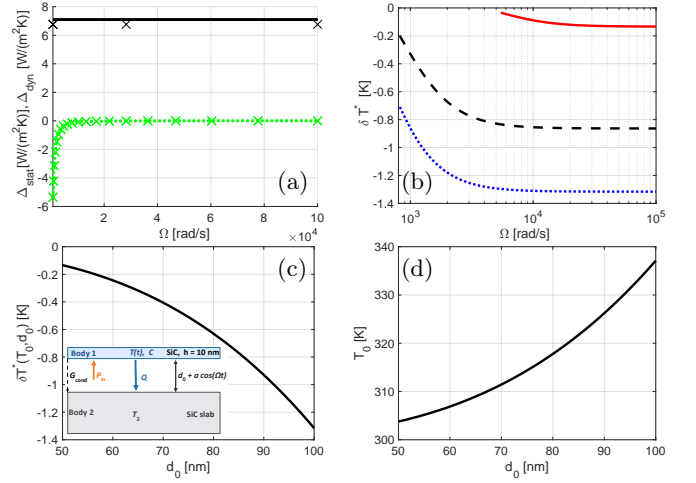


FIG. 2. (a) Static (black) and dynamic (green) Kapitza corrections versus Ω for $d_0 = 88$ nm. (b) Stationary shift δT^* versus Ω for $d_0 = 50$ nm (red), 88 nm (black), and 100 nm (blue). (c) High- Ω limit of δT^* versus d_0 . (d) Unmodulated temperature T_0 versus d_0 . Parameters: $C = 10^{-2} \text{ J m}^{-2} \text{ K}^{-1}$, $G_{\text{cond}} = 10^{-4} \text{ W m}^{-2} \text{ K}^{-1}$, $P_{\text{in}} = 2 \cdot 10^2 \text{ W m}^{-2}$, $a = 0.1 d_0$.

$$\begin{aligned} & \partial_T \Delta_{\text{dyn}}(T, \Omega)|_{(T^*, d_0)} \\ &= \frac{n^2}{4} \left(\frac{a}{d_0}\right)^2 \alpha(d_0)^2 \frac{F'(T^*)D(T^*) - F(T^*)D'(T^*)}{D(T^*)^2}, \end{aligned} \quad (25)$$

where $D'(T) = 2G(T)G'(T)$, $G'(T) = \alpha m(m-1)T^{m-2}$, and $F'(T) = \alpha m(m-1) \left[(m-2)T^{m-3}S^2 + 2T^{m-2}S(mT^{m-1}) \right] - 2m \left[(m-1)T^{m-2}SG + T^{m-1}(mT^{m-1})G + T^{m-1}SG'(T) \right]$.

VIII. NUMERICAL ESTIMATES AND EXPERIMENTAL CONSIDERATIONS

To illustrate these effects, we compute the radiative heat flux $Q(T, T_2, d)$ for two parallel SiC slabs [11, 12]: body 1 is a $h = 10$ nm membrane at $T = 320$ K, and body 2 has $h_2 = 100$ μm and $T_2 = 300$ K [see scheme in Fig 2(c)]. Fitting $Q(T, d)$ near $d_0 = 88$ nm and $T = 320$ K to (21) yields $n \approx 3.3$, $m \approx 1$, and $A \approx 4 \cdot 10^{-23} \text{ W m}^{n-2} \text{ K}^{-m}$. Using these parameters, we evaluate $\Delta_{\text{stat}}(T_0)$ and $\Delta_{\text{dyn}}(T_0, \Omega)$ [Eqs. (22), (23)] for $d_0 = 88$ nm and $a = 0.1 d_0$ [Fig. 2(a)], showing the expected low-pass behavior of Δ_{dyn} for $\Omega \gg G/C \approx 820 \text{ s}^{-1}$. With $C = 10^{-2} \text{ J m}^{-2} \text{ K}^{-1}$, $G_{\text{cond}} = 10^{-4} \text{ W m}^{-2} \text{ K}^{-1}$, and $P_{\text{in}} = 2 \cdot 10^2 \text{ W m}^{-2}$, we obtain $T_0 = 324$ K and $G(T_0, d_0) = 8.22 \text{ W m}^{-2} \text{ K}^{-1}$. The crosses in Fig. 2(a) are obtained from numerical derivatives of the exact flux (1), without relying on the power-law approximation, and in-

dicating a fair agreement with the power-law toy model.

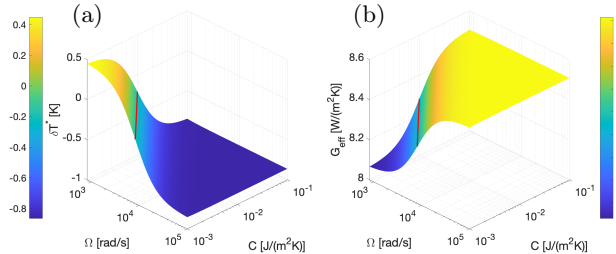


FIG. 3. (a) Slow-temperature shift δT^* and (b) effective conductance $G_{\text{eff}}(T^*, d_0, \Omega)$ versus Ω and C , for $d_0 = 88$ nm ($T_0 = 324$ K), using the same parameters as in Fig. 2. Red curves indicate the limit of validity of the averaging approximation $\Omega = G(T_0, d_0)/C$, with $G(T_0, d_0) = 8.22 \text{ Wm}^{-2}\text{K}^{-1}$.

Figure 2(b) shows the slow-temperature shift δT^* [Eq. (17)] versus Ω for three gaps, $d_0 = 50, 88, 100$ nm (with corresponding $T_0 = 303, 324, 337$ K) and $a = 0.1d_0$. As expected, δT^* is always negative and saturates at large Ω , giving $\delta T^* = -0.13$ K, -0.86 K, and -1.32 K, respectively. These shifts can be strongly amplified by increasing the input power. For instance, keeping the same power-law parameters for Q and $d_0 = 88$ nm, raising the input to $P_{\text{in}} = 2 \cdot 10^3 \text{ Wm}^{-2}$ increases the unmodulated temperature to $T_0 = 542$ K and yields a much larger Kapitza-like shift, $\delta T^* = -8.6$ K.

Figure 2(c) shows the temperature shift δT^* versus d_0 in the large- Ω limit, where $\Delta_{\text{stat}}(T_0)$ dominates. The shift decreases at short distances because, in Eq. (17), the denominator (temperature derivative) decreases more slowly than the numerator (distance derivative), given the fitted near-field power-law exponents n and m . In the far field ($n = 0, m = 4$), both Δ_{stat} and Δ_{dyn} vanish, so $\delta T^* = 0$. Figure 2(d) reports the unmodulated temperature T_0 versus d_0 .

Figure 3(a,b) displays the slow-temperature shift δT^* and the effective conductance $G_{\text{eff}}(T^*, d_0, \Omega)$ [Eq. (19)] as functions of the modulation frequency Ω and the heat capacity C , for $d_0 = 88$ nm (all parameters given in the caption). The red curve indicates $\Omega = G(T_0, d_0)/C$, marking the lower bound of the high-frequency averaging regime ($\Omega \gg G(T_0, d_0)/C$). Reducing C enhances the Kapitza-like effect.

Finally, Fig. 4 presents the full temporal dynamics of the system, with further details provided in the caption.

We note that the lumped-body approximation is well justified for our $h = 10$ nm SiC membrane: the Biot number $\text{Bi} = Gh/k \approx 7 \times 10^{-10} \ll 1$ (where $k \approx 120\text{--}490 \text{ W m}^{-1}\text{K}^{-1}$ is the SiC thermal conductivity) confirms static thermal uniformity, and the thermal penetration depth $\delta_{\text{th}} = \sqrt{2\kappa/\Omega} \approx 32 \mu\text{m}$ at $\Omega = 10^5 \text{ rad/s}$ (where $\kappa = k/(\rho c_p) \approx 5 \times 10^{-5} \text{ m}^2\text{s}^{-1}$ is the thermal diffusivity, with $\rho \approx 3210 \text{ kg m}^{-3}$ and $c_p \approx 750 \text{ J kg}^{-1}\text{K}^{-1}$) exceeds h by more than three orders of magnitude, ensuring a uniform dynamic response throughout the entire modulation frequency range considered.

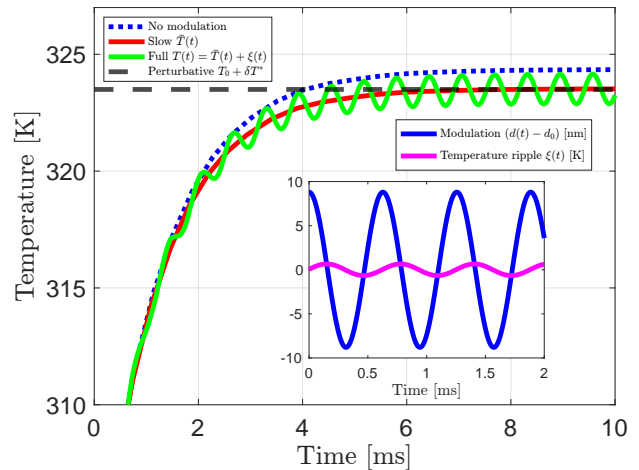


FIG. 4. Time evolution for $d_0 = 88$ nm, $\Omega = 10^4$ rad/s, and the same parameters as in Fig. 2: unmodulated steady state T_0 [(14)]; slow averaged component $\bar{T}(t)$ [(10)]; full solution $T(t) = \bar{T}(t) + \xi(t)$ [(8),(10)]; perturbative prediction $T_0 + \delta T^*$ [(16)] Inset: fast oscillations of the gap modulation $d(t) - d_0$ and the induced de-phased temperature ripple $\xi(t)$.

Promising platforms include polar dielectrics supporting surface phonon polaritons [9, 26], ultrathin suspended membranes minimizing C , and MEMS/NEMS actuators enabling stable sub-100 nm gaps [20]. The predicted shifts δT^* and changes in G_{eff} are directly measurable in suspended-membrane NFRHT experiments. A key requirement is minimizing parasitic heating from the gap-modulation actuator. For typical electrostatic MEMS/NEMS devices driven at kHz-MHz, the dissipated power per unit actuator area is in the sub-nW range, yielding a total power much smaller than the radiative flux over the same area, and can thus be safely neglected in the thermal balance. Temperatures can be read out via resistance or optical thermometry, both offering 10-50 mK resolution, well below the predicted ~ 1 K shifts. A practical protocol is to sweep the modulation frequency Ω while monitoring the slow temperature component $\bar{T}(t)$; the crossover at $\Omega \simeq G/C$ and the high- Ω saturation of δT^* provide clear signatures of the Kapitza-like averaging mechanism. These considerations indicate that the effect is well within reach of current experimental platforms.

IX. CONCLUSIONS

We have generalized the Kapitza mechanism to NFRHT, showing that rapid modulation of any flux-controlling parameter produces a universal correction to the slow thermal dynamics. The resulting closed-form dynamics reveal two contributions: a frequency-independent static term and a frequency-dependent dynamical term, which together generate a modulation-induced temperature shift and modify the effective thermal conductance. As in the Kapitza pendulum, fast driving produces an effective po-

tential; here it yields an *effective thermal conductance* that can stabilize or destabilize the temperature evolution. This mechanism can be particularly useful when the unmodulated system is only marginally thermally stable. The theory is fully general and applies to arbitrary geometries and to modulation of dielectric properties or separations, requiring only small amplitudes and a clear timescale separation. For gap modulation between two parallel slabs, we derived analytical scalings and numerically predicted temperature shifts of ≈ 1 K for ultrathin SiC membranes, with ≈ 10 K shifts readily accessible

at higher powers. We also identify a promising experimental platform for observing this effect and show that it lies within current experimental feasibility. Future investigations could explore promising platforms for implementing effective thermal-conductance stabilization in near-field systems exhibiting negative differential thermal conductance, enabled, for instance, by the metal-insulator transition of phase-change materials such as vanadium dioxide (VO_2). These results establish a thermal analogue of the Kapitza mechanism and a route to dynamic control of nanoscale thermal systems.

-
- [1] P. L. Kapitza, Dynamic stability of the pendulum with an oscillating point of suspension, *Sov. Phys. JETP* **21**, 588 (1951).
- [2] D. Kuzmanovski, J. Schmidt, N. A. Spaldin, H. M. R. Rnnow, G. Aepli, and A. V. Balatsky, Kapitza stabilization of quantum critical order, *Phys. Rev. X* **14**, 021016 (2024).
- [3] N. N. Bogoliubov and Y. A. Mitropolsky, *Asymptotic Methods in the Theory of Nonlinear Oscillations* (Gordon and Breach, New York, 1961).
- [4] L. D. Landau and E. M. Lifshitz, *Mechanics*, 3rd ed. (Butterworth-Heinemann, Oxford, 1976).
- [5] M. Bukov, L. D'Alessio, and A. Polkovnikov, Universal high-frequency behavior of periodically driven systems: from dynamical stabilization to floquet engineering, *Advances in Physics* **64**, 139 (2015), <https://doi.org/10.1080/00018732.2015.1055918>.
- [6] N. Goldman and J. Dalibard, Periodically driven quantum systems: Effective hamiltonians and engineered gauge fields, *Phys. Rev. X* **4**, 031027 (2014).
- [7] A. Eckardt, Colloquium: Atomic quantum gases in periodically driven optical lattices, *Rev. Mod. Phys.* **89**, 011004 (2017).
- [8] D. Polder and M. V. Hove, Theory of radiative heat transfer between closely spaced bodies, *Phys. Rev. B* **4**, 3303 (1971).
- [9] K. Joulain, J.-P. Mulet, F. Marquier, R. Carminati, and J.-J. Greffet, Surface electromagnetic waves thermally excited: radiative heat transfer, coherence properties and casimir forces revisited in the near field, *Surf. Sci. Rep.* **57**, 59 (2005).
- [10] B. Song, A. Fiorino, E. Meyhofer, and P. Reddy, Near-field radiative thermal transport: From theory to experiment, *AIP Advances* **5**, 053503 (2015).
- [11] R. Messina and M. Antezza, Scattering-matrix approach to casimir-lifshitz force and heat transfer out of thermal equilibrium between arbitrary bodies, *Phys. Rev. A* **84**, 042102 (2011).
- [12] B. Zhao, B. Guizal, Z. M. Zhang, S. Fan, and M. Antezza, Near-field heat transfer between graphene/hbn multilayers, *Phys. Rev. B* **95**, 245437 (2017).
- [13] S. Zhang, Y. Dang, X. Li, N. Iqbal, Y. Jin, P. K. Choudhury, M. Antezza, J. Xu, and Y. Ma, Measurement of near-field thermal radiation between multilayered metamaterials, *Phys. Rev. Appl.* **21**, 024054 (2024).
- [14] M. Lim, J. Song, S. S. Lee, and B. J. Lee, Tailoring near-field thermal radiation between metallo-dielectric multilayers using coupled surface plasmon polaritons, *Nature Communications* **9**, 4302 (2018).
- [15] J. C. Cuevas and F. J. Garcia-Vidal, Radiative heat transfer, *ACS Photonics* **5**, 3896 (2018), <https://doi.org/10.1021/acsphotonics.8b01031>.
- [16] F. Geesmann, P. Thureau, S. Rodehutsors, T. Ziehm, L. Worbes, S.-A. Biehs, and A. Kittel, Transition from near-field to extreme near-field radiative heat transfer, *Phys. Rev. Lett.* **135**, 166202 (2025).
- [17] R. S. Ottens, V. Quetschke, S. Wise, A. A. Alemi, R. Lundock, G. Mueller, D. H. Reitze, D. B. Tanner, and B. F. Whiting, Near-field radiative heat transfer between macroscopic planar surfaces, *Phys. Rev. Lett.* **107**, 014301 (2011).
- [18] K. Kim, B. Song, V. Fernández-Hurtado, W. Lee, W. Jeong, L. Cui, D. Thompson, J. Feist, M. T. H. Reid, F. J. García-Vidal, J. C. Cuevas, E. Meyhofer, and P. Reddy, Radiative heat transfer in the extreme near field, *Nature* **528**, 387 (2015).
- [19] A. Fiorino, D. Thompson, L. Zhu, B. Song, P. Reddy, and E. Meyhofer, Giant enhancement in radiative heat transfer in sub-30 nm gaps of plane parallel surfaces, *Nano Letters* **18**, 3711 (2018).
- [20] R. St-Gelais, L. Zhu, S. Fan, and M. Lipson, Near-field radiative heat transfer between parallel structures in the deep subwavelength regime, *Nature Nanotechnology* **11**, 515 (2016).
- [21] M. F. Picardi, K. N. Nimje, and G. T. Papadakis, Dynamic modulation of thermal emission—a tutorial, *J. Appl. Phys.* **133**, 111101 (2023).
- [22] R. Yu and S. Fan, Time-modulated near-field radiative heat transfer, *Proceedings of the National Academy of Sciences* **121**, e2401514121 (2024), <https://www.pnas.org/doi/pdf/10.1073/pnas.2401514121>.
- [23] Y. Sun, Y. Hu, K. Shi, J. Zhang, D. Feng, and X. Wu, Negative differential thermal conductance between weyl semimetals nanoparticles through vacuum, *Physica Scripta* **97**, 095506 (2022).
- [24] D. Feng, X. Yang, and X. Ruan, Phonon scattering engineered unconventional thermal radiation at the nanoscale, *Nano Letters* **23**, 10044 (2023), pMID: 37889143, <https://doi.org/10.1021/acs.nanolett.3c03375>.
- [25] M. Pascale, M. Giteau, and G. T. Papadakis, Perspective on near-field radiative heat transfer, *Applied Physics Letters* **122**, 100501 (2023).
- [26] S.-A. Biehs, R. Messina, P. S. Venkataram, A. W. Rodriguez, J. C. Cuevas, and P. Ben-Abdallah, Near-field radiative heat transfer in many-body systems, *Rev. Mod.*

- [Phys. **93**, 025009 \(2021\)](#).
- [27] R. St-Gelais, B. Guha, L. Zhu, S. Fan, and M. Lipson, Demonstration of strong near-field radiative heat transfer between integrated nanostructures, [Nano Letters **14**, 6971 \(2014\)](#), PMID: 25420115, <https://doi.org/10.1021/nl503236k>.
- [28] C. Lucchesi, R. Vaillon, and P.-O. Chapuis, Temperature dependence of near-field radiative heat transfer above room temperature, [Materials Today Physics **21**, 100562 \(2021\)](#).